Fabrication and biocompatibility characterization of porous alumina-hydroxyapatite composites prepared by protein foaming-consolidation method

Ahmad Fadli
Department of Chemical Engineering, Faculty of Engineering, Riau University,
Jln. HR. Subrantas, Km 12.5 Panam Pekanbaru, Riau 28293, Indonesia

Abstract

Porous alumina ceramics have been attracting considerable attention for cell loading and bone grafts. Although porous alumina provides relatively high mechanical properties in respect to bioactive porous ceramics, the bioinertness of alumina hamper its application for for permanent bone implant. On the other hand, the use of hydroxyapatite (HA) for bone surgery is highly succesful due to its biocompatibility, bioactivity and osteoconduction characteristics. Its is therefore attractive to combine the mechanial properties of alumina with the bioactive of hydroxyapatite for bone generation. This report presents fabrication and biocompatibility test of porous alumina–hydroxyapatite composites fabricated through protein foaming–consolidation technique. Alumina and sol-gel derived HA powder were mixed with yolk and starch at an adjusted ratio to make slurry. The resulting slip was poured into cylindrical shaped molds and followed by foaming and consolidation via 180°C drying for 1 h. The obtained green bodies were burned at 600°C for 1 h, followed by sintering at temperatures of 1200–1550°C for 2 h. Porous alumina–HA bodies with 26–73 vol.% shrinkage, 29%–52% porosity and 0.1–4.9 MPa compressive strength were obtained. The compressive strength of bodies increased with the increasing sintering temperatures. The addition of sol-gel derived HA in the body was found to decrease the compressive strength. Biocompatibility study of porous alumina–HA was performed in a stirred tank bioreactor using culture of Vero cells. A good compatibility of the cells to the porous microcarriers was observed as the cells attached and grew at the surface of microcarriers at 8–120 cultured hours. The cell growth on porous alumina microcarrier was 0.015 h^{-1} and increased to 0.019 h^{-1} for 0.3 w/w HA-to-alumina mass ratio and decreased again to 0.017 h^{-1} for 1.0 w/w ratio. Carbon concentration on porous alumina bodies without addition was 36.03%; it significantly increased 46.14 when 1.0 w/w HA was added.

Keywords: Cell culture, biocompatibility, alumina, microcarrier, hydroxyapatite

INTRODUCTION

Porous alumina ceramics have been attracting considerable attention for scaffold applications, especially for cell carrier and bone grafts (Eckert et al., 2000; Bieniek and Swiecki, 1991). Because of bioinert of nature of alumina, it has lack of bioactivity properties even though provides a very high mechanical properties. In addition, alumina was reported to form the thinnest fiber layer the surface compared with the other bioinert ceramics (Miao, et al., 2007). On the other hand, the uses of calcium phosphate ceramics for bone surgery are highly successful due to their biocompability, bioactivity and osteoconduction characteristics (Kang, et al., 2005; Frieβ and Warner, 2002). Hydroxyapatite (HA, $Ca_{10}(PO_4)_6(OH)_2$) and tricalcium phosphate (TCP, $Ca_3(PO_4)_2$) in porous, granular and dense forms are most commonly used calcium phosphate-based bioceramics in bone regeneration. Even though HA and TCP have similar chemical composition, they differ in their biological resorbing

capacity. The HA when used as bone implant is almost non-resorbable in body fluid while TCP is relatively soluble and is used as bio-cements or bone filler (Best, et al., 2008).

Various methods on fabricating porous alumina compositized with calcium phosphate have been developed. Jun et al. (2003) fabricated alumina porous bodies using the polyurethane sponge and the calcium phosphate were coated onto the porous alumina substrates. This techniques resulted porous bodies with 90-75% porosity and compressive strength of up to 6 MPa. In vivo test also shown that the HA-coated alumina porous implants had a similar bioactivity and osteoconduction property to the HA porous implant. Saki et al. have developed composite ceramic bioscaffold of hydroxyapatite-alumina by using an organic template which is commercial polyurethane sponge with an open interconnected microporosity. It has good properties which exhibit better biodegradability, light in weight and can support osteoblast attachment and growth as well. The process starts with preparation of slurry (HA, and alumina) and polyurethane sponge is then immersed in the slurry and finally the sample put in furnace for sintering process. Osteoblast-like cells cultured on the scaffold and their growth pattern is observed. This scaffolds morphology shown fairly uniform pores with size range between 2.5-5 μm and cell growth shows that the scaffolds is able to support the osteoblast attachment and growth (Saki, et al., 2009).

Previously, we have successfully manufactured porous alumina ceramics through protein foaming-consolidation method using egg yolk as pore creating agent. The advantage of this method is pore creation can be done at very low temperature (110-180˚C) compared conventional methods (500-600°C) (Gregorova and Pabst, 2007; Wang, et al., 2006; Isobe, et al., 2007; Prabhakaran, et al., 2007; Lyckfeldt and Ferreira, 1998). In direct protein foaming method which egg white protein was used, pore generation by foaming is achieved in stirring or milling followed by drying its consolidation or gelation only take place (Dhara and Bhargava, 2003; Garrn, et al., 2004), whereas in our work, both the foaming and consolidating occured in drying. Therefore, control of porosity can be achieved by controlling the composition of the slurry in the earlier method and by composition of slurry and drying temperature as well in our work. This work suggested that egg yolk delayed foaming during stirring. The lipids phase in egg yolk would lessen the foaming capacity of protein in creating pores (Lomakina and Mikova, 2005).

In this paper, porous alumina-HA composite developed via protein foaming-consolidation method are presented. The microcarriers were applied for cell culture in a spinner vessel bioreactor.

METHODOLOGY

Materials

A commercial alumina powder (Sigma-Aldrich, USA), with an average particle size of 0.25 μm and a specific surface area of 0.39 m^2/g was used. The HA powder prepared by sol-gel method was used in the experiment. Protein used was yolk that freshly isolated from chicken egg (LTK Berhad, Malaysia). Castor oil (Sigma Aldrich, USA) was used as the lubricant for facilitating demolding Starch flour (FFM Berhad, Malaysia) was chosen as binder. Darvan 821 A (40 wt.% aqueous solution of ammonium polyacrylate; R.T. Vanderbilt, USA) was selected as the dispersant. Calcium nitrate tetrahydrate (Systerm, Malaysia), di-ammonium hydrogen phosphate (Systerm, Malaysia), ammonium solution (Systerm, Malaysia) and urea (Systerm, Malaysia), Titriplex II (Merck, German) were used to produce sol-gel derived HA powder.

Synthesis of sol-gel derived HA powder

Sol-gel derived HA powder was synthesized using calcium nitrate tetrahydrate and di-ammonium hydrogen phosphate as the precursor for calcium and phosphorus respectively. The sol-gel method employed in this work was adapted from the procedure developed by Bezzi et al (2002). A 500 mL of ammonium solution (25%) was heated at 60°C, 182 g of Titriplex II was added while stirring until it dissolved and gave clear solution. Into this, 200 mL of aqueous solution of 130 g of $Ca(NO_3)_2.4H_2O$ was poured, and then 40 g of $(NH_4)_2HPO_4$ and 45.2 g of urea were subsequently added. The mixture was then refluxed while stirring until a white gel of HA was obtained. The obtained gel was then dried under ambient air and subsequently subjected to heat treatment under flowing air.

Fabrication of alumina-HA and alumina TCP composite porous bodies

The alumina-HA composite porous bodies were prepared using protein foaming-consolidation method. The slurries were prepared by stirring the alumina powder (24 g and 10 g), sol-gel derived HA (3.2 g – 10.0 g) , yolk (24 g), starch (4 g) and Darvan 821 A in a beaker glass. The amount of Darvan 821 added was restricted to a level to maintain the slurry flowable for casting. The slurries were mechanically stirred (Heidolph, RZR 2052 control model) at 150 rpm for 3 h in ambient environment. Subsequently, the slurries were cast in cylindrical open stainless steel mold with 10.75 mm diameter and 15.10 mm height and dried in an air oven (Memmert, 100-800 Model) at temperature of 180°C for 1 hour. Castor oil was used as lubricant for easy mould removal and led to better surface qualities. Finally, the dried samples were burned in a furnace (Protherm, PLF 160/5 Model) at rate of $10°Cmin^{-1}$ up to 600°C for removal of the yolks and then sintered at rate of $2°Cmin^{-1}$ up to 1200°C - 1550°C for 2 h.

.

Characterization

The particle size of powder was measured using a Nanosizer (Malvern, ZEN1600 model). An electronic densimeter (Alfa Mirage, MD300S model) was used to measure the apparent density of sintered porous composite samples. The total porosity of the samples was considered by measuring its dimension and density. The crystallinity of the sintered porous samples was analyzed by XRD (Shimadzu, XRD-6000) using Cu Ka radiation at 30 mA, 40 kV. Surface morphology of sintered samples was examined using SEM (JEOL, 5600 model) and FESEM (JEOL, JSM 6700 F model). Compressive strength was measured using a universal testing machine (Lloyd, LR10K plus model) by diametrical compression at a loading rate of 2.5 mm min^{-1} on the samples of 8 mm diameter and 10 mm height. Five scaffolds were used to determine the average value of each compressive test.

Biocompatibility tests

The samples with spherical shape with with a diameter of 6 mm were used. The Vero cells were grown in 75 cm^2 culture T-flaks at 37°C and 5% CO_2 into 15 mL fresh Dulbecco's Modified Eagle's Medium (DMEM) supplemented with 10% Fetal Bovine Serum (FBS). Aseptic technique has been employed during the sampling. Sampling was conducted every twelve hours for 120 hours. It was done by taking out 1 mL sample of each spinner vessel culture and the number of viable cells was counted to observe the remaining number of suspended cells by using the inverted microscope. The sampling is necessary to infer the cell attachment on the porous microcarries. The specimens were fixed with 4% Glutaraldehyde for 30 min and dehydrated in solutions containing ethanol of various concentrations (10%,

30%, 50%, 70%, 90%, 100%) before drying in the air oven overnight at 37°C. FESEM measurement was conducted for the cell morphology analysis.

RESULTS AND DISCUSSIONS

Characteristics of HA powder

The sol-gel derived HA showed nanometric primary particles of about 75-150 nm with globular shapes in the particles. The morphology of nano powder had effect on densification, microstructure and mechanical peroperties (Banerjee et al., 2007).

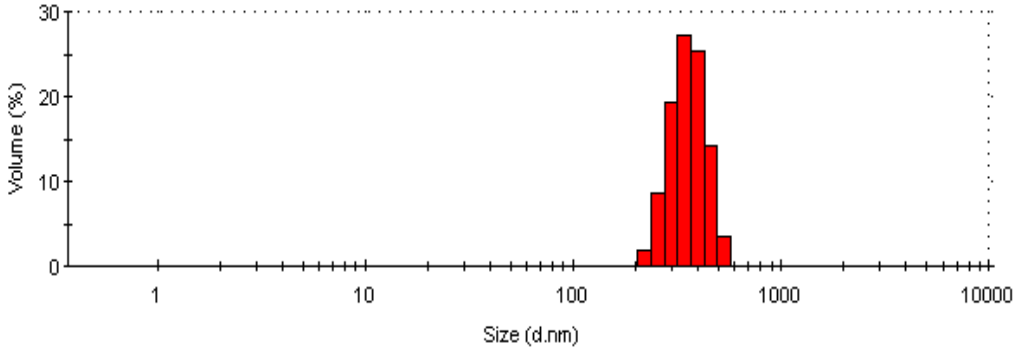

Figure 14.6. Particle size distribution graph of sol-gel derived hydroxyapatite

The particle size measured in a Dynamic Light Scattering (DLS) instrument is the diameter of the sphere that diffuses at the same speed as the particle being measured. The average particle for sol-gel derived HA was 562.1 nm.

Rheology behaviors of slurry

Slip casting is one of the most common forming techniques used in the fabrication of ceramics. To obtain successful casting results, concentrated slurry with good rheological properties was needed. The ideal slurry should have the highest solids loading with the lowest viscosity. The high solids loading help to reduce the shrinkage and related cracking. The low viscosity or high flowability enhances the molding process (Bose et al., 2002). The measurement of slurries rheological in this work were conducted at shear rates from 10 to 450 s^{-1} at ambient temperature.

The measurement of slurries rheological in this work were conducted at shear rates from 10 to 450 s^{-1} at ambient temperature. Figure 2 shows the influence of yolk addition on viscosity of slurry within 3 h after mixing. It can be seen clearly that addition of yolk resulted in a significant increases in viscosity over the shear rate considered. A viscosity as high as 16.55 Pa s was observed for the slurry containing 34 g yolk at low shear rate (10 s^{-1}) but it decreased significantly to 2.24 Pa s when the 64 g yolk was added (slurry S24). The viscosity value of the all slurries at higher shear rate (450 s^{-1}) was in the range 1.25 – 1.29 Pa s indicating that the slurries are pourable under shear. The slurries containing lower yolk amount were pseudoplastic in behavior and it shifted to Newtonian fluid when yolk concentration was increased.

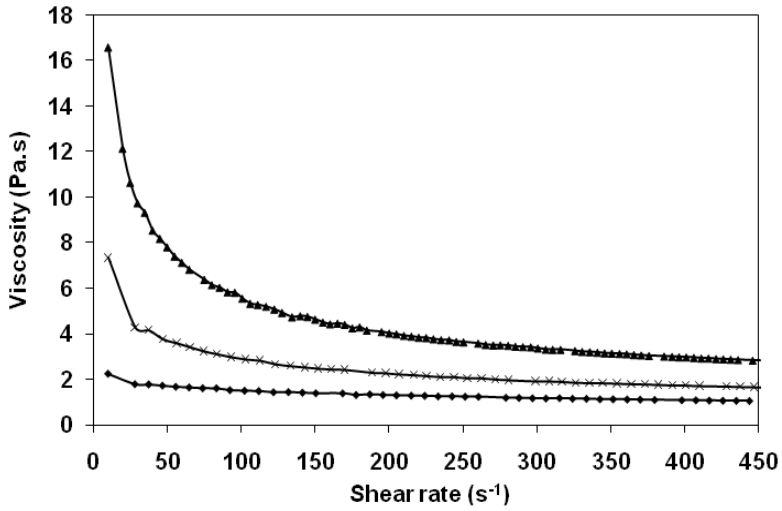

Figure 2. Rheological curves of slurries with different yolk content (34 g, 44 g and 64 g)

The pseudoplasticity of slurries can be characterized by non-Newtonian index n calculated according to the power law model. The calculated n index for slurry containing 34 g, 44 g, and 64 g are 0.5, 0.6 and 0.8, respectively. Whereas, the calculated k values for all slurries are 47.2, 15.8 and 4.4, respectively.

The Physical properties of porous bodies

After stirring process, the slurries were cast in cylindrical moulds and then heated in an air oven at 180°C for 1 h undergo both foaming and consolidation method. The green bodies have sufficient strength for removal from the mould and for further handling. The bottom and upper parts of green bodies were cut to obtain fine cylindrical shape.

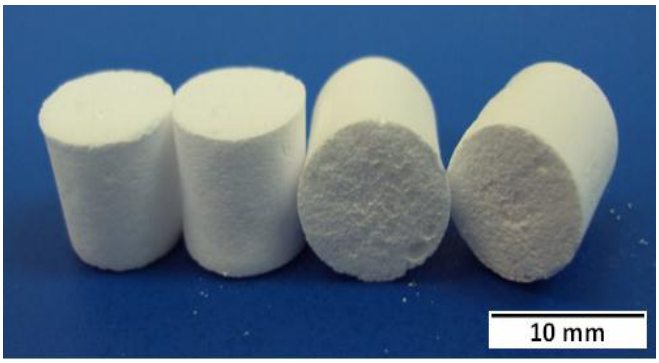

Figure 4. The porous alumina-HA composite with cylindrical shape

Figure 4 shows a photograph of four sintered porous alumina-HA composite bodies with cylindrical shape. The bodies did not show any deformation or cracks during burn out of pore former and sintering.

Foaming-consolidation process

To evaluate mechanism of slurry foaming during drying process, the slurry was investigated. The evolution of foaming capacity versus the drying time of slurry is shown in Figure 5. Foaming of slurry took place in four steps: pre-heating, foaming, consolidating and stabilizing steps. In the pre-heating step i.e at 2 min drying time, the structural properties of protein changed (so-called denaturation) by heating without increase in volume.

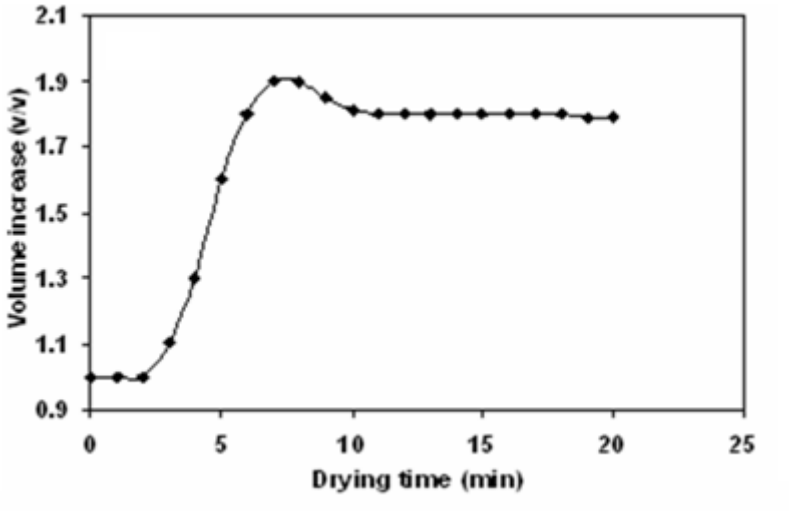

Figure 5. Increasing volume of slurry during drying process

Subsequently when the drying time increased from 3 to 7 min, the slurry was strongly foaming as reflected by a drastic increase in volume until it reaches the maximum value. The increasing volume was originated from foaming ability of protein in the slurry. At drying time of 8 to 11 min, the yolk formed gel network structure which it is attributed to its constituent protein denaturation, leading to molecular consolidation and the development of a rubbery-like slurry. In the consolidating process the drying body comprises solid and liquid phases. The body is bounded by a gaseous interface. The liquid evaporates into this gaseous phase and is transferred away from drying body by diffusion or convection. Evaporation will be determined by the difference in liquid vapor pressure at the surface and the ambient vapor pressure, as well as the rate at which the air is flowing across the surface. In the limit of slow evaporation, the volume of drying body is reaching minimum (Brown and Zukoski, 2002). No change in volume of the body was observed after 11 min drying (stabilizing stage). The stability of foam was achieved after the body dried more than 20 min. The slurry started to foam at the centre of cast slurry and then the foaming capacity significantly increased with time until a constant volume is reached. The bodies also show an increasing pore size with drying time.

Effect of sintering temperature on the physical properties

To investigate effect of sintering temperature on the physical properties of porous bodies prepared using sol-gel derived HA were evaluated. The mechanical properties of a porous material depend on the porosity as suggested by Gibson and Ashby (1997). Because porosity decreased with the increase of sintering temperature, the compressive strength should increase with the increase of sintering temperature.

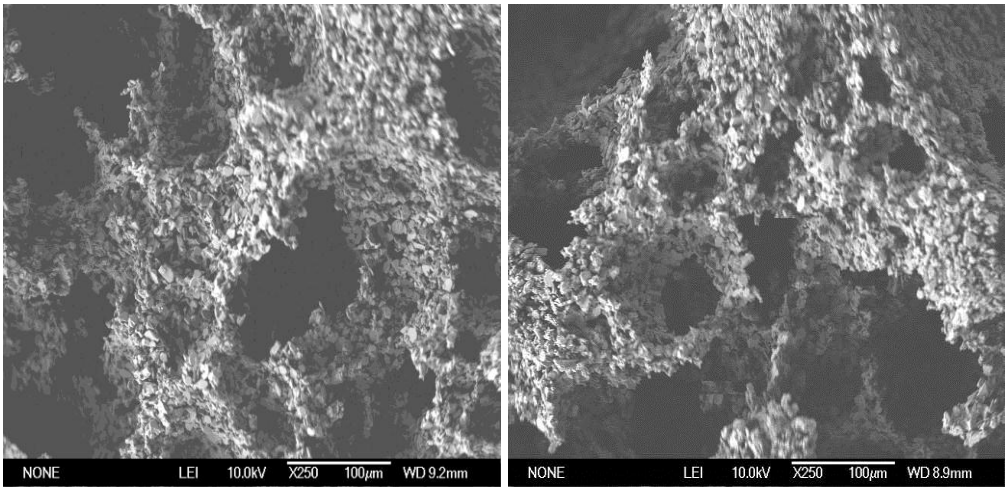

Figure 6. The macrostructures of bodies after sintered at (a) 1350 and (b) 1550°C

Figure 6 show the macrostructure of the samples sintered at 1350 and 1550°C. The increase sintering temperature resulted in smaller pore size and denser struts. It can explain that, the shrinkage increase with sintering temperature, thus the pore sizes would decrease as well. Banerjee et.al confirmed that nanostructured material can improve the sinterability due to high surface energy and, therefore, improve mechanical properties. But sintering behavior not only depends on particle size but also on particle size distribution and morphology of the powder particles. Large particles size along with hard agglomerates exhibits lower densification in HA. Difference in shrinkage between the agglomerates is also responsible to produce small cracks in the sintered HA. Therefore, synthesis of the agglomerate free step to achieve good mechanical properties for dense nanostructure (Banarjee, et al., 2007).

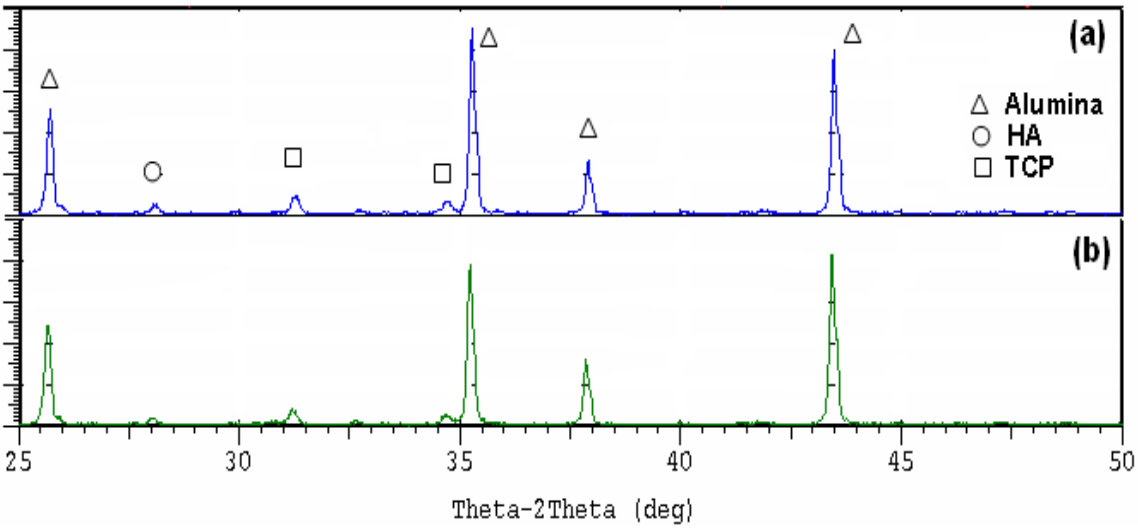

Figure 7. XRD pattern of porous alumina-hydroxyapatite bodies after sintered at (a) 1350 and (b) 1550°C

To evaluate the effect of sintering temperature on crystalinnity, samples with sintering temperatures of 1350°C and 1550°C were compared. Figure 7 shows XRD peaks of porous

alumina-hydroxyapatite composite sintered at 1350°C and 1550°C. In addition, the crystallinity of HA and TCP of 1550°C sintering temperature was lower than the crystallinity of HA and TCP of 1350°C sintering temperature. Moreover, no additional phase identified among the two patterns. This indicates that the sintering process does not change the composition of the porous composite.

Effect of solid loading on the physical properties

The influence of HAs amount in slurry on mechanical strength was investigated using sintered samples prepared from slurries with different composition. Figure 8 and Figure 9 display the EDX map of area in porous body for different samples. The distribution of both alumina and HAs phases could be identified based on color of wall surface of body. The white color area of sample with highest HA atom peak was confirmed as HA phase (Fig.ure 8), whereas dark grey area with highest alumina atom peak was confirmed as alumina as shown in Figure 9.

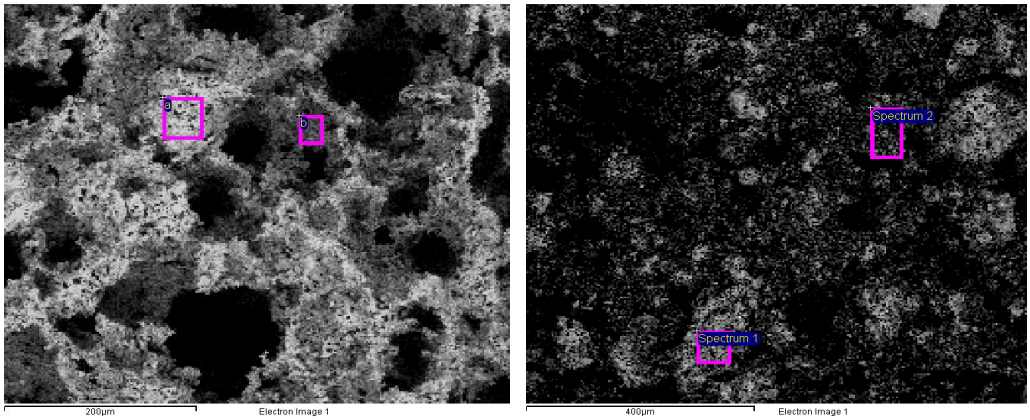

Figure 8. EDX analysis of porous body with HA-to-alumina mass ratio of (a) 3.0 and (b) 1.0 w/w

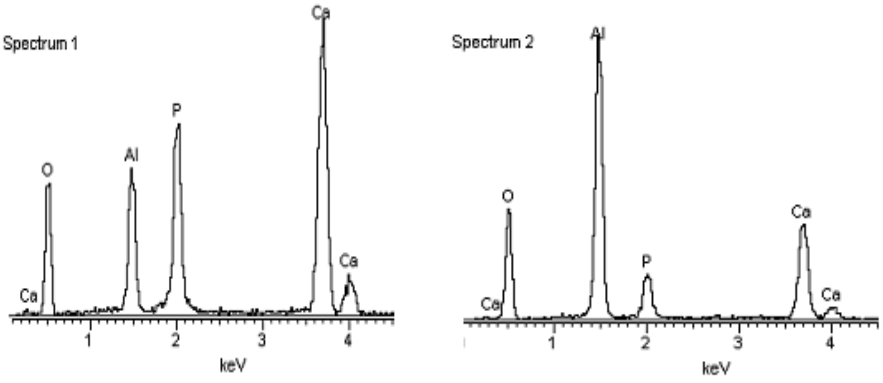

Figure 9. EDX peaks of (a) white area and (b) dark grey areas element analysis

The increasing HA content decreases compressive strength at constant sintering temperature. A compressive strength as high as 2.18 MPa was found for the sample containing 0.3 w/w HA-to-alumina mass ratio, but it decreased to 0.56 MPa when mass ratio

was increased to 0.5 w/w. Further addition of HA up to 1.0 w/w mass ratio have decreased compressive strength of samples reach 0.15 MPa. The addition of HA powders decrease grain size of particles of body's walls. At 0.3 w/w mass ratio the particles are more bonding area among grains. More bonding area usually leads to higher strength between particles. The higher strength between particles would result in higher strength of samples because the fracture of alumina-HA composites mainly happens at the particles boundary.

Sintering of HA is complicated by the fact that HA is hydrated phase that decomposes to anhydrous calcium phosphates such as TCP at ~1200 – 1450˚C. Decomposition results from dehydroxylation beyond a critical point. For temperatures below the critical point (1300˚C), the HA crystal structure is retained despite dehydroxylation, and then the HA rehydrates on cooling. If the critical point is exceeded, complete and irreversible dehydroxylation occurs, resulting in collapse of the HA structure and decomposition. After the critical point α-TCP and β-TCP are often formed. The increasing HA added increases shrinkage and compressive strength but decreasing porosity. At sintering temperatures above 1200°C, HA become unstables and forms decomposed phases such as α-tricalcium phosphate (α-TCP), β-TCP, tetracalcium phosphate (TTCP) and calcium oxide. It is well known that the solubility of TCP is much higher than that of HA. It is believed that HA reacts with alumina at the HA/alumina interface during heat treatment and some of the HA decomposed to TCP (Banarjee et al, 2007). During sintering process at 1550°C, the HA and TCP particles would melt and result in smaller pore size and denser walls, eventually increasing shrinkage degree. The shrinkage increases from 76.7 to 83.5 vol.% when HA loading was increased from 4 to 8 g. The nanostructured HA powder can improve the sinterability due to higher surface energy and, therefore, improves mechanical properties. For the decreased porosity from 45.8 to 36.8%, the compressive strength increased from 2.9 to 20.4 MPa.

The shrinkage of porous bodies decrease from 70.10% at HAs-to-alumina mass ratio of 0.3 w/w is 70.10% to 48.65% at 1.0 w/w's ratio. Conversely, the addition of HAc would improve shrinkage of the bodies and obtained in the range of 76.7-83.5. Whereas the decreasing alumina amount from 15 to 10 g led to increasing shrinkage from 64.4 to 76.7 Vol.% and decreasing porosity from 34.9 to 45.8%. In fact, even though the porosity of bodies decreases with reducing alumina loading the compressive strength also decreases.

Micro-CT scan

Traditional methods of visualizing the microstructure of composites as well as other materials involve simplifying the three dimensional (3D) structure to a two-dimensional (2D) representation by optical or scanning electron microscope (SEM). While 2D representation of microstructures is common and gives some idea of the microstructure morphology, it is not fully representative of the 3D structure of the material. While visualization of the 3D microstructures of the material is important, prediction of the behavior and properties of the materials is equally important. A micro-CT imaging images allow for non destructive 3D imaging of the mass distribution of real objects. Absorption tomography is based on the detection of radiation attenuated by an object for many different angular positions.

Figure 10 shows Micro-CT images of samples cross section of HA thickness with color coding for different HA loading. The thickness of HA increased with increasing HA loading in slurry. Dissimilarity in HA distribution was found in samples. For sample containing 0.3 w/w HA-to-alumina mass ratio showed that the middle part of porous body had higher HA concentration than the upper part (Figure 10a). On the other hand, in the 1.0 w/w HA-to-alumina mass ratio sample the HA particles tend to precipitate in the surface part as shown in Figure 10b.

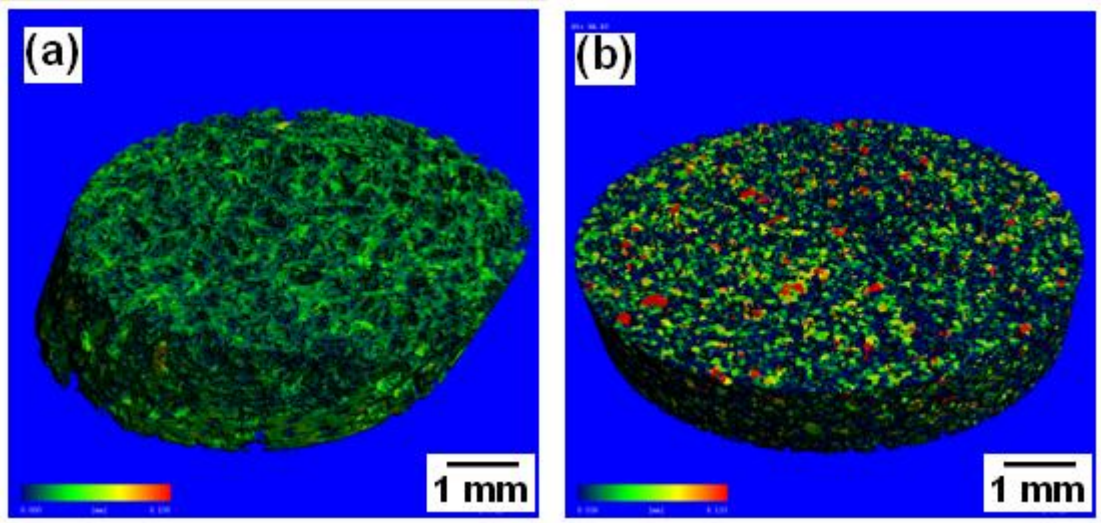

Figure 10. Micro CT images of bodies with HA-to-alumina mass ratio (a) 0.30 and (b) 1.00 w/w

Figures of 10 shows whole 3D images of pores with color coding for different HA content. The addition of HA amount in slurry resulted big in the pore size. The pore sizes of body prepared using slurry containing 0.3 w/w HA-to-alumina mass ratio were found in the range 0 – 0.46 mm (Figure 10b), whereas pore size of 1.0 w/w mass ratio's body were in the range 0 – 0.32 mm (Figure 10b). Even though maximum pore size of the samples was almost same i.e 0.13 mm, but number of counts of the size significantly different. Number of 0.3 mm pore size for 0.3 w/w mass ratio sample was 1,700,000, whereas for 1.0 w/w mass ratio sample was 5,000,000.

Growth of Vero cells in Bioreactor

In order to evaluate the biocompatibility of porous alumina-HA composites prepared the samples were applied as microcarriers for Vero cells culture in a stirred tank bioreactor. The stirred tank bioreactor was used for cell culture due to its simplicity and ease of monitoring and controlling of growth (Warnock and Al-Rubeai, 2005). Porous alumina samples without HA addition were tested also for comparison. Inoculums for porous alumina samples were 4.8×10^4 cells/mL, whereas for porous alumina-HA composites with 0.3 and 1.0 w/w ratios, 8.6×10^4 cells/mL inoculums were seeded. The cell observation attached on all microcarriers was done every 12 hours.

It was found that all Vero cells grew well on all samples. The cells with size in the range 20 to 30 µm would attach to the external surface of the alumina-HA composite microcarriers and grow in to the internal pores with 20 to 250 µm diameters, thus being protected from mechanical damage. The cells can break due to fluid dynamic generated stresses, which may arise from agitation and aeration and it is commonly called 'shear damage'. There are three potential damage mechanism to the cells; collision among cell-covered microcarriers; collision with parts of the reactor (especially the impeller); and interaction with turbulent eddies. If the stirring speeds were too high, cells would detach from microcarriers, particularly during mitosis; and if speeds were too low, the microcarriers did not circulate in the medium and cell growth was poor (Ibrahim and Nienow, 2004). Low agitation speed provided the highest Vero cell densities for cultivation of Vero cells on microporous and macroporous microcarriers (Souza et al., 2007). Therefore the agitation speed of bioreactor set in these studies was 35 rpm to avoid cell damaged by the impeller

speed. Besides the porous alumina-HA composites with mechanical strength in the range 0.2 to 6.4 MPa can reduce mechanical damage of microcarriers by body-body and body-impeller impacts.

Figure 11 shows the attached cells profile that revealed the VERO cell behavior. The number of cells on samples increases with incubation time. The initial attachment has a significant impact on further cell proliferation and increased cell density from day one to day four during the culture (Kong et al., 1999). After 12 hours cultivation time, the concentration of Vero cell attached on porous alumina at ratio of 0.3 w/w ratio and 1.0 w/w porous alumina-HA samples were 4 x 10^5, 3 x 10^5, 5 x 10^5 cells/mL. Increasing the HA content in samples resulted in the higher attached cells number. In reality, for porous alumina samples when cultivation time increases from 12 to 24 hours the number cells decreases from 4 x 10^5 to 1 x 10^5 cells/mL. It indicated that cells need longer time to adapt to bioinert microcarrier surface, hence the number of live cell decreased. Beyond 24 cultured hours, the cells have acclimatized with environment of microcarriers, therefore the number of cells increased again to 4 x 10^5 cells/mL.

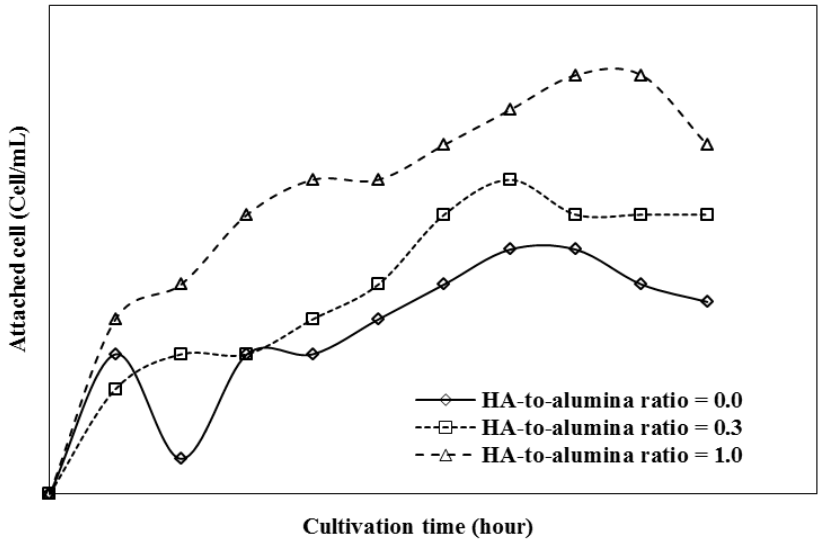

Figure 11. Attached cell profile, showing the biocompatible nature of the samples with different HA-to-alumina mass ratio

After 24 hours of cultivated time, the cell number attached on the surface of porous alumina-HA was bigger than porous alumina without HA content. Whereas cell number with low HA content was smaller than porous alumina with high concentration. It indicated that HA addition as bioactive ceramics in samples would increase cell attachment on samples' surface. The maximum cell number on surface of porous alumina containing 1.0 w/w was observed at 96 hours cultivation time.

Specific growth (μ) rate was determined as acceleration phase and microcarrier with 0.3 w/w HA-to-alumina mass ratio has the highest specific growth rate which is 0.019 h^{-1} followed by 1.0 w/w HA-to-alumina mass ratio microcarrier (μ = 0.017 h^{-1}) and porous alumina without HA addition (μ = 0.015 h^{-1}). The results for Vero cells growth kinetic on each microcarriers are shown in Figure 12.

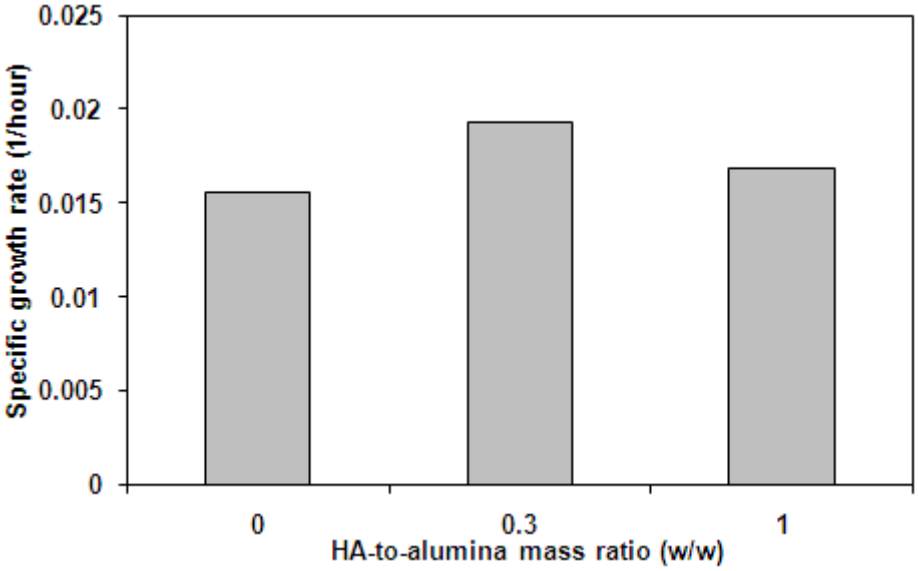

Figure 12. Specific growth rate vs HA-to-alumina mass ratio

Although microcarrier with 1.0 w/w HA-to-alumina mass ratio obtained the highest attached cells number which is 1.5 x 10^5 cells/mL, its cell growth rate was less than 0.3 w/w mass ratio microcarrier. It is indicated that the growth rate of cells was not only influenced by composition of microcarriers but also by surface morphology of the microcarriers. The pore size of 0.3 w/w microcarrier was bigger than 1.0 w/w mass ratio microcarrier.

The cell metabolism in bioreactor is supported by bigger pore size of microcarrier, thus the attached cell on surface of microcarrier pores increased. Landi et al (2006) reported that cell behavior in terms of adhesion, proliferation and metabolic activation was able to be influenced by the chemico-physical properties of the introduced powders. The lactic acid in media can devastate the surface of microcarriers and induce cell death, reducing the overall cell density and viability. For that reason usage of porous alumina-HA composites is very valuable to avoid the damage of microcarrier surfaces.

CONCLUSION

Porous alumina-hydroxyapatite composite was manufactured to improve the bioactivity while maintaining the mechanical strength of alumina ceramics via protein foaming-consolidation technique. The use of different yolk concentration in slurries affected the rheological conditions, which resulted in changes in the foaming capacity of the slurries. The compressive strength of sintered porous alumina hydroxyapatite obtained by this method was 2.9 - 20.4 MPa, and it depend on porosity of bodies. Depending on slurry composition in the slurry, the sintered body have open, interconnected porous structure with pore size of 95-300 μm. When the sintering temperatures increased from 1350 to 1550°C, the porous bodies shrunk increasingly lead to the porosity decreasing. With the increase of sintering temperature, the grain size of samples grew up, which lead to the improvement of body strength. XRD results show that crystallinity of porous bodies decreases with the increasing sintering temperatures the phase of the bodies remain unchanged. The number of attached Vero cells on sample surface increases with the increasing incubation time. The HA addition in samples would increase cell number attached on surface samples. SEM analysis of cultured cells showed a good compatibility of the Vero cells to all the porous microcarriers, since the cells were observed already attached at the surface of microcarriers at hours 8 and 120 of

incubation time. The cell growth rates of microcarriers containing 0.0, 0.3 and 1.0 w/w were 0.015, 0.019 and 0.017 $hour^{-1}$, respectively. The EDS images show that carbon content on porous alumina bodies without HA addition was 36.03%, it significantly increased 46.14% when 1.0 w/w HA was added.

REFERENCES

Bose, S., Darsell, J., Hosick, H.L, Yang, L., Sarkar, D.K., & Bandyopadhyay, A. (2002). Processing and characterization of porous alumina scaffolds. *Journal of Materials Science: Materials in Medicine, 13,* 23-28.

Brown, L.A., & Zukoski, C.F. (2002). Consolidation during drying of aggregated suspensions. *AIChE Journal, 48* (30), 492-501.

Dhara, S., & Bhargava, P. (2003). A simple direct casting route to ceramic foams, *Journal of the American Ceramic Society, 86*(10), 1645-1650.

Eckert, K.L., Mathey, M., Mayer, J., Homberger, F.R., Thomann, P.E., Groscurth, P., & Wintermantel, E. (2000). Preparation and in vivo testing of porous alumina ceramics for cell carrier applications. *Biomaterials, 21,* 63-69.

Frieβ, W., & Warner, J. (2002). Biomedical applications. In F. Schuth, K.S.W. Sing & J. Weikamp (Eds.), *Handbook of Porous Solids* (pp. 2923-2970). Weinheim, Germany: Wiley-VCH.

Garrn, I., Reetz, C., Brandes, N., Kroh, L.W., & Schubert, H. (2004). Clot-forming: the use of proteins as binders for producing ceramic foams. *Journal of the European Ceramic Society, 24,* 579-587.

Gibson, L.J., & Ashby, M.F. (Eds.). (1997). Cellular solids, structure and properties, Cambridge solid state science series. Cambridge, UK: Cambridge University Press.

Gregorova, E., & Pabst, W. (2007a). Porosity and pore size control in starch consolidation method casting of oxide ceramics-Achievements and problems. *Journal of the European Ceramic Society, 22,* 669-672.

Ibrahim, S., & Nienow, A.W. (2004). Suspension of microcarriers for cell culture with axial flow impellers. *Trans IChemE. Part A, Chemical Engineering Research and Design, 82*(A9), 1082-1088.

Isobe, T., Kameshima, Y., Nakajima, A., & Ikoda, K. (2007a). Preparation and properties of porous alumina ceramics with uni-directionally oriented pores by extrusion method using a plastic substance as a pore former. *Journal of the European Ceramic Society, 27,* 61-67.

Jun, Y., Kim, W., Kweon, O., & Hong, S. (2003). The fabrication and biochemical evaluation of alumina reinforced calcium phosphate porous implants. *Biomaterials, 24,* 3731-3739.

Kang, I., Kim, T., Ko, K., Song, H., Goto, T., & Lee, B. (2005). Microstructure and osteoblast adhesion of continuously porous Al_2O_3 body fabricated by fibrous monolithic process. *Materials Letters, 59,* 69-73.

Landi, E., Tampieri, A., Belmonte, M.M., Celotti, G., Sandri, M., Gigante, A., Fava, P., Biagini, G., & Logroscino, G. (2006). Biomimetic Mg- and Mg, CO_3- substituted hydroxyapatites: synthesis characterization and in vitro behavior. *Journal of the European Ceramic Society, 26,* 2593-2601.

Lyckfeldt, O., & Ferreira, J.M.F. (1998). Processing of porous ceramics by 'starch consolidation'. *Journal of the European Ceramic Society, 18,* 131-140.

Lomakina, K., & Mikova, K. (2005). A study of the factors affecting the foaming properties of egg white – a review. *Czech Journal of Food Science, 24,* 110-118.

Miao, X., Hu, Y., Liu, J., & Huang, X. (2007). Hydroxyapatite coating on porous zirconia. *Materials Science and Engineering C, 27*, 257-261.

Prabhakaran, K., Ananthakumar, S., & Pavithran, C. (2001). Effect of hydrolysed aluminium treatment on rheological characteristics of α–alumina slurries. *Journal of Materials Science, 36*, 4827-4831.

Prabhakaran, K., Melkeri, A., Gokhale, N.M., & Sharma, S.C. (2007). Preparation of macroporous alumina ceramics using wheat particles as gelling and pore forming agent. *Ceramics International, 33*, 77-81.

Ramay, H.R., & Zhang, M. (2003). Preparation of porous hydroxyapatite scaffolds by combination of the gel-casting and polymer sponge method. *Biomaterials, 24*, 3293-3302.

Saki, M., Narbat, M.K., Samadikuchaksaraei, A., Ghafouri, H.B., & Gorjipour, F. (2009). Biocompability study of a hydroxyapatite-alumina and silicon carbide composite scaffold for bone tissue engineering. *Yakhteh, 11*(1), 55-60.

Wang, X., Dong, P., & Chen, S. (2006). Preparation of Macroporous Al_2O_3 by Template Method. *Acta Physico-Chimica Sinica, 22*(7), 831-835.

Warnock, J., & Al-Rubeai, M. (2005). Production of biologics from animal cell cultures. In V. Nedovic and R. Willaert, *Applications of Cell Immobilisation Biotechnology* (pp. 423-438). Dordrecht, Netherlands: Springer.